



This is a repository copy of *Enhancing the seismic performance of historic timber buildings in Asia by applying super-elastic alloy to a Chinese complex bracket system* .

White Rose Research Online URL for this paper:

<https://eprints.whiterose.ac.uk/124944/>

Version: Accepted Version

---

**Article:**

Xie, W., Araki, Y. and Chang, W.-S. orcid.org/0000-0002-2218-001X (2018) Enhancing the seismic performance of historic timber buildings in Asia by applying super-elastic alloy to a Chinese complex bracket system. *International Journal of Architectural Heritage: conservation, analysis, and restoration*, 12 (4). pp. 734-748. ISSN 1558-3058

<https://doi.org/10.1080/15583058.2018.1442528>

---

**Reuse**

Items deposited in White Rose Research Online are protected by copyright, with all rights reserved unless indicated otherwise. They may be downloaded and/or printed for private study, or other acts as permitted by national copyright laws. The publisher or other rights holders may allow further reproduction and re-use of the full text version. This is indicated by the licence information on the White Rose Research Online record for the item.

**Takedown**

If you consider content in White Rose Research Online to be in breach of UK law, please notify us by emailing [eprints@whiterose.ac.uk](mailto:eprints@whiterose.ac.uk) including the URL of the record and the reason for the withdrawal request.



[eprints@whiterose.ac.uk](mailto:eprints@whiterose.ac.uk)  
<https://eprints.whiterose.ac.uk/>

# Enhancing the Seismic Performance of Historic Timber Buildings in Asia by applying Super-Elastic Alloy to a Chinese Complex Bracket System

Wenjun Xie, Yoshikazu Araki, Wen-Shao Chang

## Abstract

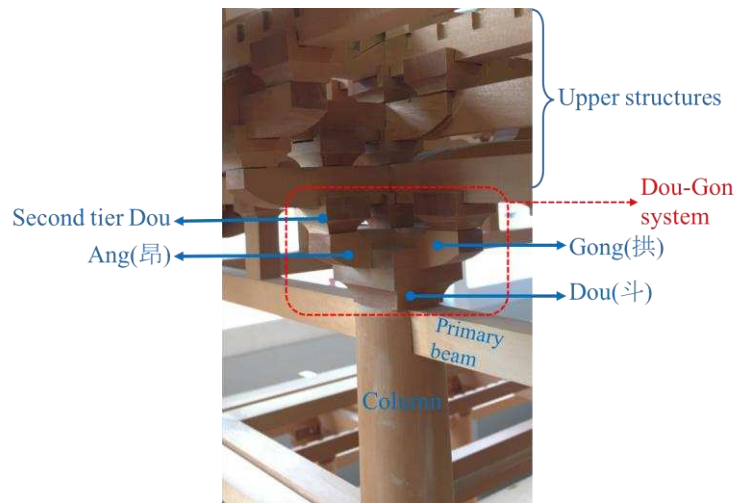
Historic timber structures that are widely distributed in East Asia are suffering from the earthquakes. This research is aiming to develop a technique to enhance the seismic performance of historic timber buildings with Dou-Gon system. High strength steel bars and super-elastic alloy bars have been used instead of the conventional wood peg connection to connect the base Dou and the column. Pushover tests have been done under all loading conditions. The energy dissipation capacity and the ultimate strength of the base Dou-Gon system have been increased by this simple technique. Base Dou-Gon system with super-elastic alloy bar connection shows a better anti-seismic performance due to its constant damping behaviour and longer fatigue life. Moreover, pre-strain of the super-elastic alloy bar can give a better damping behaviour to the base Dou system.

## 1. Introduction

Historic timber buildings such as temples, palace halls, and residential houses are widely distributed in East Asia. Most of densely distributed locations of such buildings lie in the seismic belts in East Asia, and hence there is an urgent demand for implementing protection measures against earthquakes. To this end, a significant research effort has been devoted, especially from the late 1990s, to assess the seismic performance of historic timber buildings (Fang, et al., 2001a; Fang, et al., 2001b; Suzuki & Maeno, 2006; Yu, et al., 2008; Xue, et al., 2015).

One of the primary structural components of historic timber buildings is an interlocking bracket complex, shown in Figure 1, called *Dou-Gon* in Chinese. Dou-Gon is located on top of a column to support a beam, and it transmits the vertical load of the upper frame and the roof to the column. Dou-Gon is composed mainly of the *Dou*, *Gong*, and *Ang* elements. Dou is a rectangular timber element with a cross groove at its upper side. Gong and Ang are timber

29 elements placed onto the cross groove of Dou. The base Dou sits on the top of a column, and  
30 wood pegs are used to connect the base Dou to the column.



31  
32 Figure 1 Details of Dou-Gon system

33 The nonlinear nature of the restoring force of Dou-Gon has been investigated through static  
34 and dynamic experiments (Fujita, 2000; Suzuki, 2006; Kyuke, 2008; Tsuwa, 2008; Yu, 2008;  
35 Xue, 2015; Yeo, 2016a; Yeo, 2016b) and dynamic simulations (D’Ayala, 2008; Tsai, 2011). It  
36 has been pointed out that Dou-Gon dissipates significant amount of energy mainly due to  
37 sliding between wood elements and yielding of wood elements in compression perpendicular  
38 to the grain (Fujita, 2000; Kyuke, 2008; Xue, 2015; Yeo, 2016a; Yeo, 2016b). Tsuwa et al.  
39 (2008) and Yeo et al. (2016) derived formulations for predicting the skeleton curve of the  
40 restoring force from the compression tests perpendicular to grain. D’Ayala et al. (2008) and  
41 Tsai (2011) performed nonlinear time history analysis to assess the vulnerability of historic  
42 timber buildings with the Dou-Gon system, and pointed out the necessity of improving their  
43 seismic performance.

44 Through such research works, the scientific knowledge has been improved significantly on the  
45 restoring force mechanism of Dou-Gon and its influence on overall response of a building. On  
46 the other hand, the research efforts have been scarcely seen on the techniques for enhancing  
47 the seismic performance of historic timber buildings with the Dou-Gon system.

48 Re-centring capability and energy dissipation capacity are the two fundamental characteristics  
49 that Dou-Gon system have, to give historic timber buildings good seismic performance. Re-  
50 centring capability can pull the oblique structures back to center and energy dissipate capacity  
51 will dissipate the major seismic energy. However, the conventional connectors of Dou-Gon,  
52 wood pegs, have a low ultimate strength which cause the damages of the building during

53 earthquakes. It is important to introduce a technique to enhance the Dou-Gon system by  
54 keeping the original re-centring capability and increasing the energy dissipation capacity and  
55 therefore to increase the ultimate strength and equivalent damping ratio of the structure.

56 This paper employs a simple technique to enhance the seismic performance of Dou-Gon using  
57 metal bars. With the use of metal bars, the proposed technique attempts to increase stiffness,  
58 strength, and energy dissipation of the Dou-Gon system. Static tests are performed to assess  
59 the restoring force curve of a Dou-Gon system whose base Dou is connected to the wood base  
60 using steel and super-elastic alloy (SEA, which is also been known as shape memory alloy)  
61 bars. Simple formulations are also derived for estimating the strength of the Dou-Gon system  
62 with and without the metal bars.

63

## 64 **2. Methods**

65 This study used glued laminated timber (glulam) to build a full-scale base Dou system that  
66 duplicates an ancient structure in Sichuan Province in China. Pushover tests have been  
67 performed to obtain the load-rotation curves of base Dou with different connections of  
68 conventional wood pegs, steel bars and SEA bars. The lateral loads are applied by a hydraulic  
69 jack manually. The ultimate strength and energy dissipation capacity of each test condition can  
70 be estimated to evaluate the seismic performance of the base Dou system.

### 71 **2.1. Specimen Preparation**

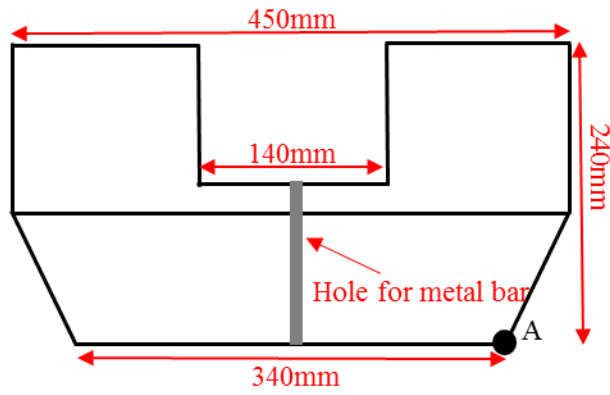
72 The base Dou is the Dou that sits on the top of a column in structures. In this paper, the base  
73 Dou was made by glulam of the strength class GL28h (Table 1) and its dimensions are  
74 illustrated in Figure 2. It was connected by three different materials (wood peg, high strength  
75 steel bar and SEA bar) to a timber block with the dimensions of 400x400x200mm (Figure 3).  
76 The timber block was fixed by two 24mm threaded bolts to the strong floor. One Gong and one  
77 Ang were fitted in the groove of the base Dou (Figure 4). A pallet with several wood bricks  
78 (shaded area in Figure 11) was fixed at their bottom to the top of the base element to fit the  
79 irregular top surface of the base Dou system. Several concrete blocks were pre-casted and put  
80 onto pallet to apply the vertical loads to the system.

81 Table 1 Mechanical properties of glulam GL28h, MPa (reference?)

Mean modulus of elasticity in bending ( $E_{0,\text{mean}}$ )	12600
Mean modulus of elasticity perpendicular to grain ( $E_{90,\text{mean}}$ )	420
Bending strength ( $f_{m,k}$ )	28

Tension strength parallel to grain ( $f_{t,0,k}$ )	19.5
Compression strength parallel to grain ( $f_{c,0,k}$ )	26.5
Compression strength perpendicular to grain ( $f_{c,90,k}$ )	3.0

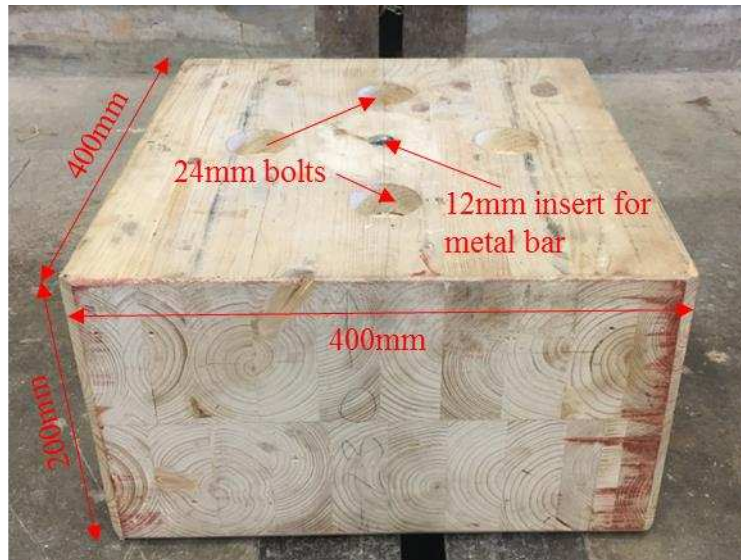
82



83

84

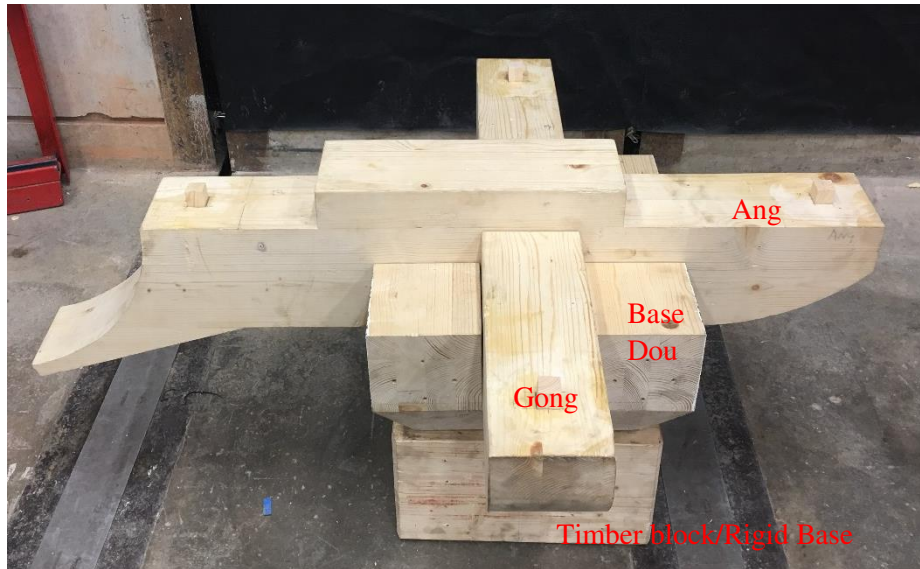
Figure 2 The section of base Dou



85

86

Figure 3 The timber block that fix the base Dou to the ground

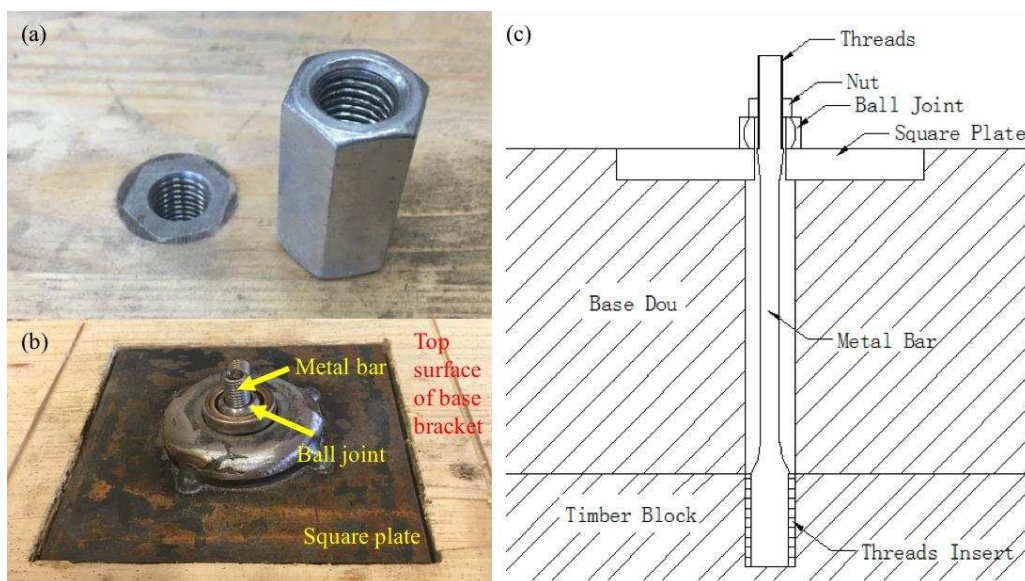


87

88

Figure 4 Dou-Gon set up without loads

89 A 12mm threads insert (Figure 5a) was fixed into the timber block with epoxy resin. A vertical  
 90 hole was pre-drilled at the centre of the base Dou. Either high strength steel or SEA bar with  
 91 threads was installed through the vertical hole of the base Dou and connected to the insert. A  
 92 square steel plate with length of 100mm was embedded into the top surface of the base Dou to  
 93 bear the pre-load applied to the bar and prevent damaging of the timber. A ball joint was  
 94 installed at the top of the bar to remove the rotational restraint from the connection system. A  
 95 nut was introduced to fix the connection system and provide pre-loading to the connection  
 96 system in some cases. Details of the metal bar connecting technique can be seen from Figure  
 97 5b and 5c.



98

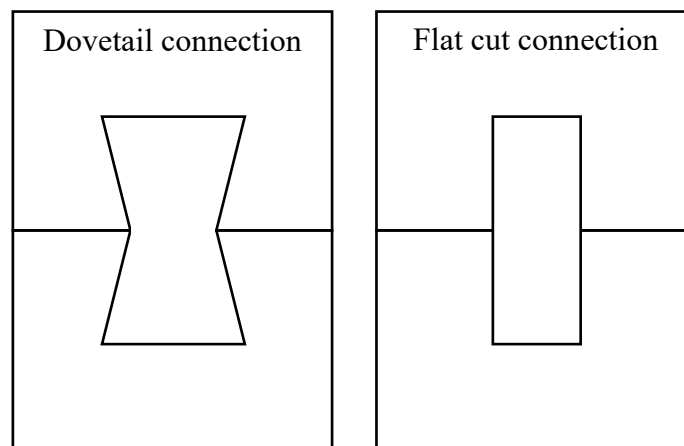
99 Figure 5(a) 12mm threads insert; (b) Square plate and ball joint; (c) Details of metal bar connection



100

## 101 2.2. Materials for the Connection

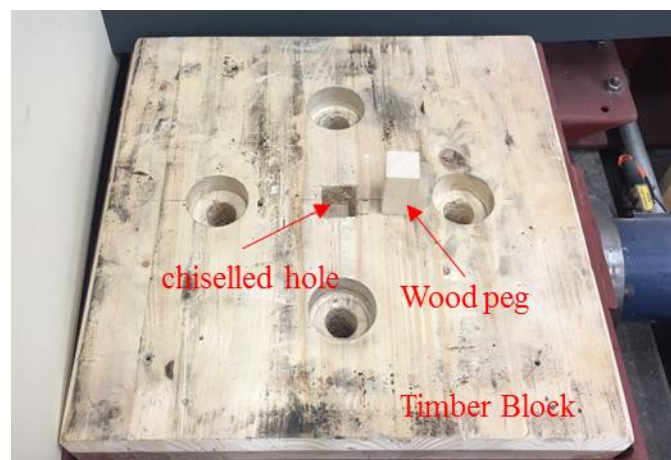
102 Wood pegs are the conventional connectors used in traditional timber structures to connect the  
103 components in the Dou-Gon system. Dovetail and flat cut (Figure 6) are the two different types  
104 of timber connections. When the connection is dovetailed, the pull out force will not be affected  
105 by the vertical load, whereas the pull out force is dependent on the vertical load with the flat  
106 cut connection (D'Ayala, 2008).



107  
108

Figure 6 Dovetail and flat cut connections

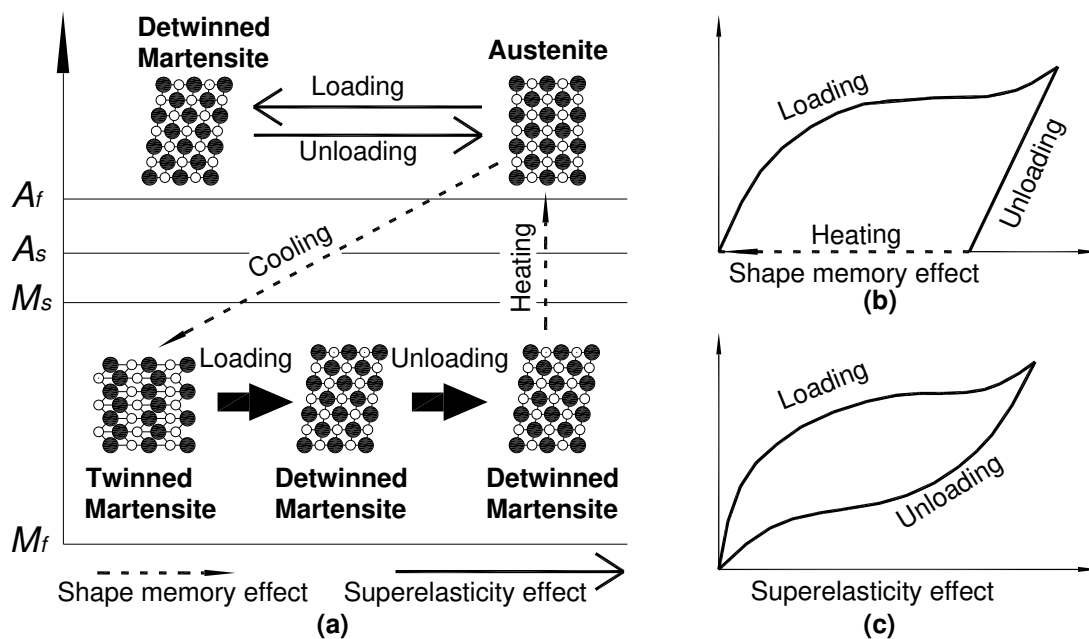
109 In this research, flat cut wood peg connection was employed. The timber grade of the peg is  
110 the same as Dou-Gon. The width of the wood pegs used in this research is one fifth of the width  
111 of the groove and the dimensions are 28x28x56mm. Cubic holes with the width of 28mm were  
112 chiselled out in both bottom of the Dou and top of the timber block respectively to install the  
113 wood peg (Figure 7).



114  
115

Figure 7 Wood peg and chiselled hole

116 To enhance the structural behaviour of the Dou-Gon system, the super-elastic alloy bar was  
 117 employed instead of the wood peg connection. The super-elastic alloy is well-known as shape  
 118 memory alloy (SMA) due to its shape memory effect. Shape memory alloy (SMA) is a metallic  
 119 material with two main crystal structures, martensite and austenite which depends on  
 120 temperature and external stress. The former phase is the low temperature phase whereas the  
 121 latter one is the high temperature phase. There are four temperatures referring to the phase  
 122 transformation,  $M_f$ ,  $M_s$ ,  $A_s$  and  $A_f$  in an ascending order.  $M_s$  and  $M_f$  are the start and finish  
 123 temperature points of the martensite phase and  $A_s$  and  $A_f$  are the start and finish transformation  
 124 temperatures from martensite phase back to austenite phase (Janke, et al., 2005). The shape  
 125 memory effect is that crystal structure of SMA will transfer from twinned martensite to  
 126 detwinned martensite by applying external stress in the temperature range of  $M_s$  and  $M_f$ . In this  
 127 research, the material has super-elastic effect because the  $A_f$  of the material is much lower than  
 128 the ambient temperature. The interconversion between the detwinned martensite and austenite  
 129 phases will occur under loading-unloading condition. Therefore, in this paper, they have been  
 130 referred to as super-elastic alloy to distinguish them from the ones with shape memory effect.  
 131 The nature of SMA/SEA is schematized in Figure 8 (Chang & Araki, 2016).

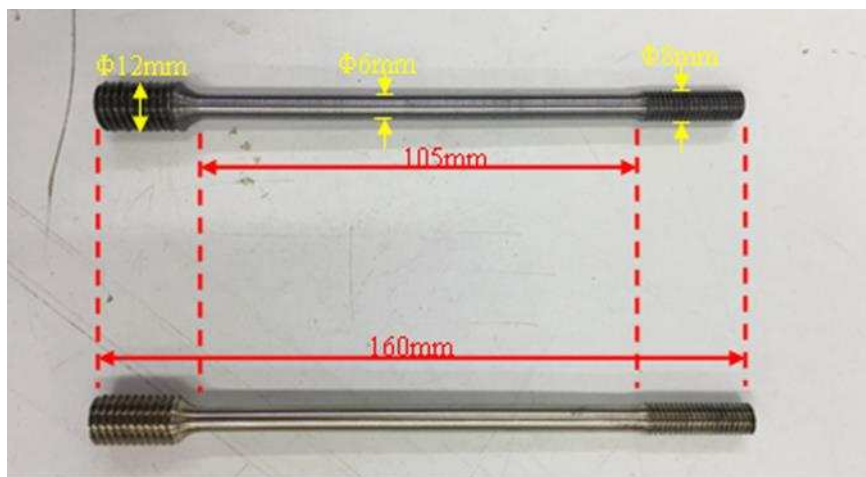


132  
 133 Figure 8 The different phases of SEA in different temperature, and its relation with the shape memory  
 134 and superelasticity effects (Chang & Araki, 2016)

135 Not only the SEA bars, high strength steel bars were also used instead of the wood peg  
 136 connection as a comparative parameter (Figure 9). The high strength steel bar has an ultimate  
 137 tensile strength of 720MPa and SEA bar has the ultimate tensile strength of 200MPa. The SEA



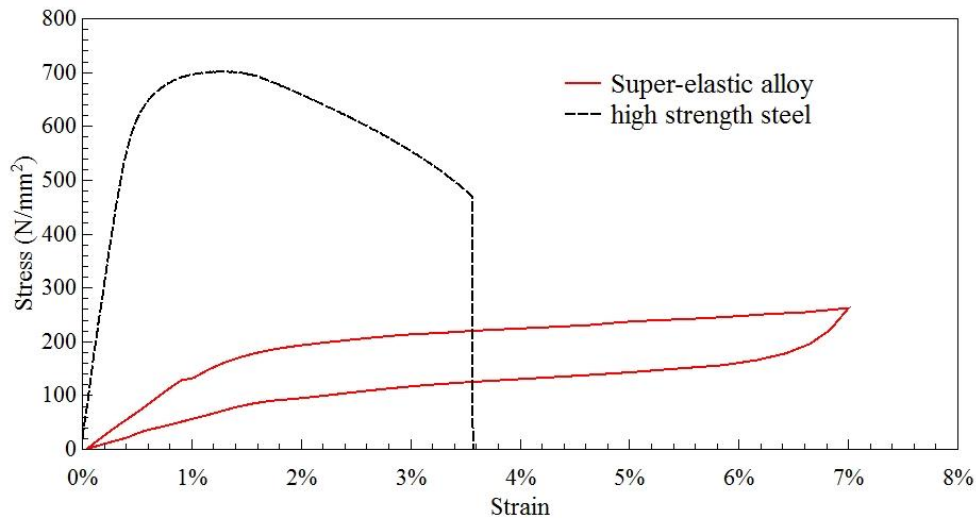
138 used in this research have the chemical composites that measured by a Scanning Electron  
139 Microscope of copper (81.84wt%), aluminium (7.43wt%) and manganese (10.74wt%). (Araki,  
140 2011; Omori, 2013) They are provided by Furukawa Techno Material Co., Ltd., Japan. The  
141 transformation temperature,  $A_f$ , is  $-39\text{ }^\circ\text{C}$ ; much lower than the normal ambient temperature  
142 that gives a stable super-elastic behaviour to the material. Both materials have an initial  
143 diameter of 12mm. The length of the specimens is 160mm. There are M8 and M12 threads at  
144 the two ends of the specimens as shown in Figure 9. The middle part of the specimens was  
145 machined down to 6mm diameter to reduce the risk that Dou will be damaged by the large pre-  
146 strain load. The length of the reduced section part is 105mm. The tensile stress-strain curves of  
147 both high strength steel bar and SEA bar are illustrated in Figure 10. The ultimate tensile  
148 strength of high strength steel bar is much higher than the SEA bar. But it was fractured at  
149 3.6% strain. The SEA bar was pulled to 7% strain and there is negligible residual strain after  
150 unloading.



151

152

Figure 9 High strength steel bar (top) and SEA bar (bottom)



153

154

Figure 10 Stress-strain curves of metal bars

155

### 156 3. Experimental Programme

157 To simulate the weight of the roof supported by the Dou-Gon system, the vertical loads of three  
 158 different load levels (4kN, 7kN and 10kN) were applied to the top of the specimen using  
 159 concrete blocks. The specimen was rotated around point A in Figure 2 by applying a lateral  
 160 load at a height of 500mm to the bottom surface of the base Dou (Figure 11) using a hydraulic  
 161 jack. It recovered to its original position when the lateral load is released. The trajectory of the  
 162 specimen which rotates to a certain point with prescribed radian ( $\theta$ ) and recovers to its original  
 163 position is defined as one loading cycle. The specimens were tested under static cyclic loadings.  
 164 Four vertical LVDTs (No 1 to 4) were used to record the rotation of the Dou and two horizontal  
 165 LVDTs (No. 5 and 6) were used record the horizontal displacement of the specimen as depicted  
 166 in Figure 11. The radians ( $\theta$ ) are worked out by the differences in measurements ( $\Delta L$ ) between  
 167 LVDT 1&2/3&4.

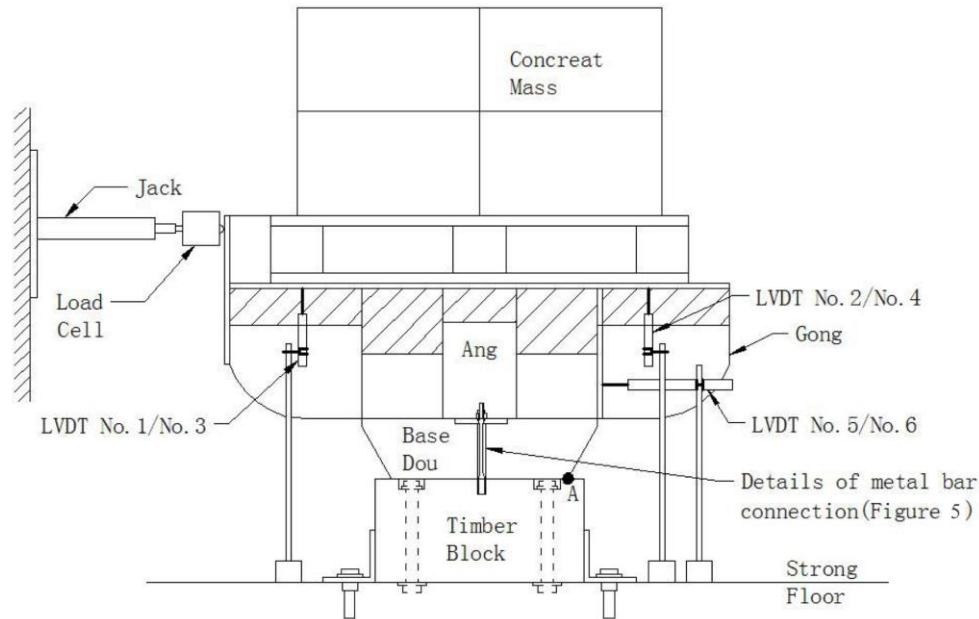


Figure 11 Loading apparatus and instrumentation used

168  
169

170 In addition to the non-prestrain conditions, the Cu-Al-Mn SEA bars were pre-strained by  
 171 stretching along the bar axis at 1%, 3% and 5% strains using a nut. The SEA bar with 1% pre-  
 172 strain condition was tested under three different vertical loads 4kN, 7kN and 10kN. The SMA  
 173 bar with 3% and 5% pre-strain conditions was tested under 10kN vertical load only. Table 2  
 174 lists all the test conditions.

175 Table 2 Experimental conditions

Connector Material	Vertical Loads (kN)		
	4kN	7kN	10kN
Wood Peg	✓	✓	✓
High Strength Steel Bar	✓	✓	✓
SMA Bar	✓	✓	✓
SEA Bar with 1% pre-strain	✓	✓	✓
SEA Bar with 3% pre-strain			✓
SEA Bar with 5% pre-strain			✓

176 Generally, all specimens were rotated up to when  $\Delta L$  is 80mm with 10mm increment. The  
 177 specimens with steel bar connection experienced 3 loading cycles when  $\Delta L$  equals to 60mm  
 178 and was loaded 10 cycles in total. For the specimens with SEA bar connection, it was loaded 2  
 179 cycles at  $\Delta L = 70$ mm when the SEA bar has 0% pre-strain under 10kN vertical loads and only  
 180 1 loading cycle for each prescribed rotations with other SEA bar connection conditions. The  
 181 specimens with wood peg connections were tested for only one loading cycle with  $\theta = 10\%$ . The  
 182 actual setup can be seen in Figure 12.

183 Table 3 Loading conditions

$\Delta L(\text{mm})$	High Strength Steel Bar Connections	SEA Bar Connection with 0% pre-strain under 10kN vertical load	Other SEA Bar Connections
10	1 cycle	1 cycle	1 cycle
20	1 cycle	1 cycle	1 cycle
30	1 cycle	1 cycle	1 cycle
40	1 cycle	1 cycle	1 cycle
50	1 cycle	1 cycle	1 cycle
60	3 cycles	1 cycle	1 cycle
70	1 cycle	2 cycles	1 cycle
80	1 cycle	1 cycle	1 cycle

184



185

186

Figure 12 The test setup of Dou-Gon with 10kN dead load

187

## 4. Results and discussions

188

### 4.1. Base Dou system with conventional wood peg connector

189

The specimens with wood peg connectors have been tested for one loading cycle with  $\theta=10\%$ .

190

The hysteresis loops (Figure 13) illustrated the non-linear restoring force of the Dou-Gon

191

system with conventional wood peg connector. Three stages of stiffness could be discovered

192

from the hysteresis loops, the elastic, plastic and limit stages (Yu, 2008). The elastic stage has

193

a high stiffness which is independent of the vertical loads. The applied lateral load increases

194

rapidly until reaching the yield point. At the plastic stage, the wood peg connection began to

195

bear the shear and flexural moments and was pulled out from the chiselled hole as the lateral

196

load increased to reach the limit rotation. The ultimate strength and the second stiffness of the

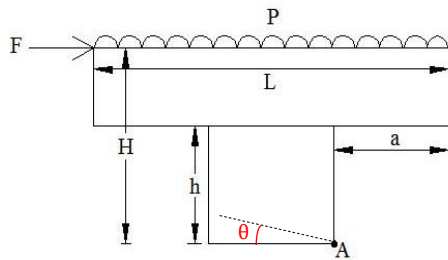
197

base Dou system increased significantly with the vertical loads. Higher vertical loads made a

201 greater contribution to the P-Delta effect which results in a lower limit stiffness of the base  
 202 Dou system. The restoring force of the structure with wood peg connection can be calculated  
 203 as:

$$204 \quad F = \frac{P \times \cos \theta}{L \times H} \left( aL - 2a^2 - 2ah \times \tan \theta - \frac{h^2 \times \tan^2 \theta}{2} \right) \quad (1)$$

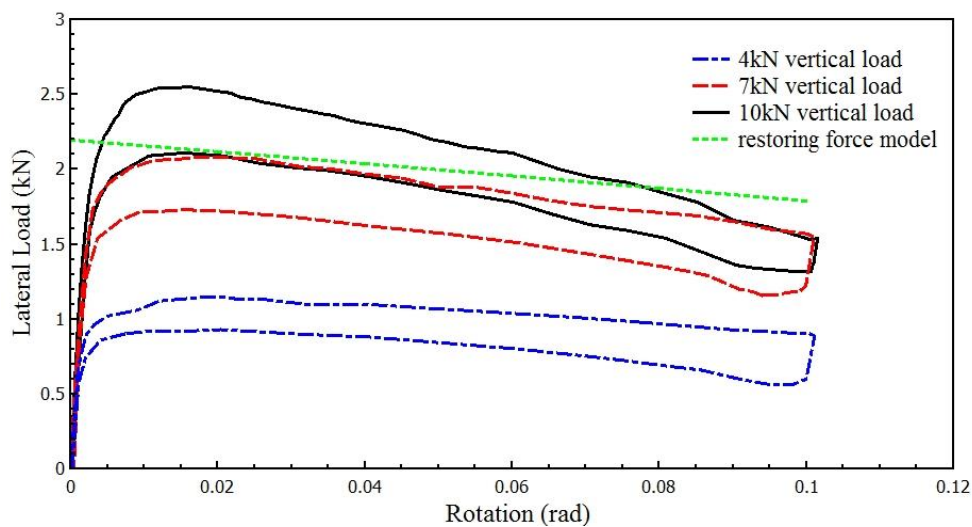
205 where P is the vertical load, L, H, a and h are illustrated in



206 Figure 14.

207 The equation also expresses that the restoring force will increase with increasing the vertical  
 208 load applied on the top of the Dou-Gon system. The restoring force curve obtained using the  
 209 restoring force model is shown in Figure 13 when the vertical load is 10kN.

210 The energy dissipation is the energy loss per loading cycle which is represented by area  
 211 enclosed by each hysteresis loop. The energy dissipation of Dou-Gon with a wood peg  
 212 connection (Table 4) has a significant rise when the vertical loads increased from 4kN to 7kN  
 213 and remain constant when the vertical loads reached 10kN. The base Dou system with  
 conventional wood peg connection shows a full re-centring capability as expected because the  
 system came back to its original position without any sliding after unloading.



214 Figure 13 The first cycle hysteresis loop of Dou-Gon with wood peg connection  
 215

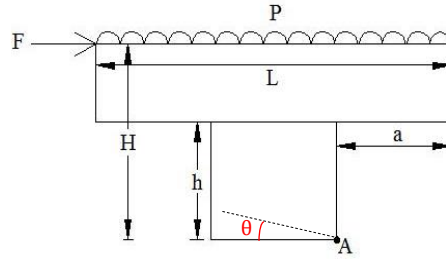


Figure 14 Simplified model of the structure and loadings

216  
217

218 Table 4 The energy dissipation of Dou-Gon system with a wood peg connection

Vertical Loads (kN)	4	7	10
Energy dissipation (N.rad)	23.8	34.7	34.9

## 219 4.2. Behaviour of base Dou system with different vertical connectors

220 The hysteresis loops of the Dou-Gon system with connectors made of 3 different materials and  
 221 under 3 different vertical loads are illustrated in Figure 15 to Figure 17. The figures clearly  
 222 show that the Dou-Gon itself already has a good re-centering capability with wood peg  
 223 connector and the re-centring force was given by the vertical loads representing the heavy roof  
 224 weight. Such re-centering characteristics are also seen in the literature (Suzuki, 2006; Yu,  
 225 2008).

226 The base Dou system with SEA bar connection has experienced four stages stiffness. The first  
 227 two stiffness are the stiffness of the timber structure since there was little gap between the  
 228 structure and the connection system. The lateral load needs to overcome the vertical loads until  
 229 the SEA bar starts to work. So, the third and fourth stiffness are the stiffness of the entire system.  
 230 The restoring force curves reproduce the base Dou system with SEA bar connection and  
 231 showed a good matching with the experimental results for 4kN and 7kN dead load levels, while  
 232 ayield load higher than the experimental yield force was observed for the 10kN dead load. The  
 233 restoring force of the structure with SEA bar connection can be calculated as:

$$234 \quad F = \frac{P \times \cos \theta}{L \times H} \left( aL - 2a^2 - 2ah \times \tan \theta - \frac{h^2 \times \tan^2 \theta}{2} \right) + \frac{k_1 \left( \frac{L}{2} - a \right)^2 \sin \theta}{H} \quad (2)$$

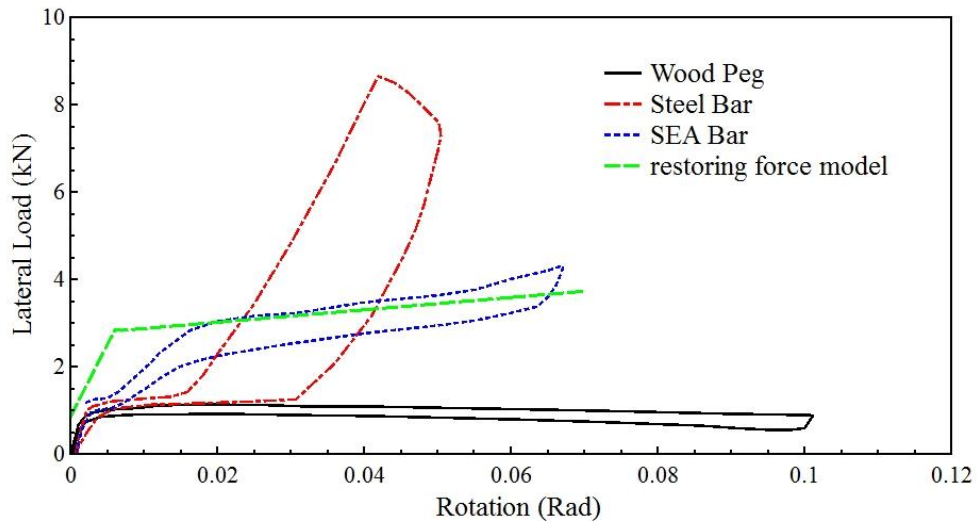
235 when  $\theta \leq 0.59\%$ ;

$$236 \quad F = \frac{P \times \cos \theta}{L \times H} \left( aL - 2a^2 - 2ah \times \tan \theta - \frac{h^2 \times \tan^2 \theta}{2} \right) + \frac{k_2 \left( \frac{L}{2} - a \right)^2 \sin \theta + A \left( \frac{L}{2} + a \right)}{H} \quad (3)$$

237 when  $\theta > 0.59\%$ .  $k_1$  and  $k_2$  are the tensile stiffness of SEA bar.

238

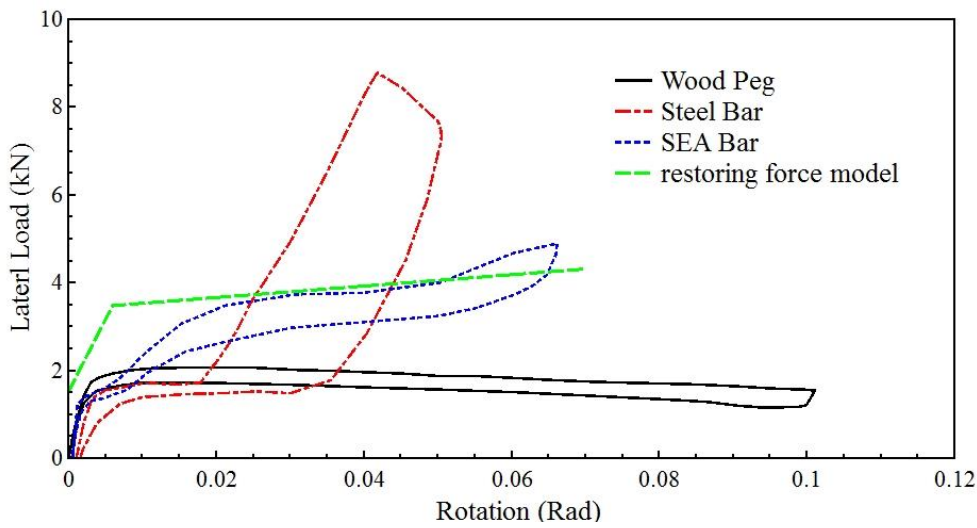




239

240

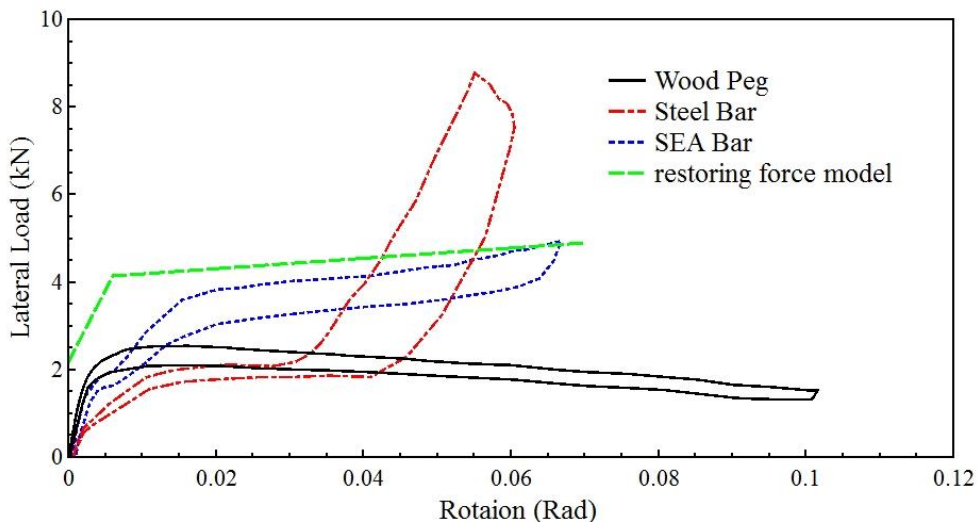
Figure 15 The second cycle hysteresis loops of Dou-Gon under 4kN dead load



241

242

Figure 16 The second cycle hysteresis loops of Dou-Gon under 7kN dead load



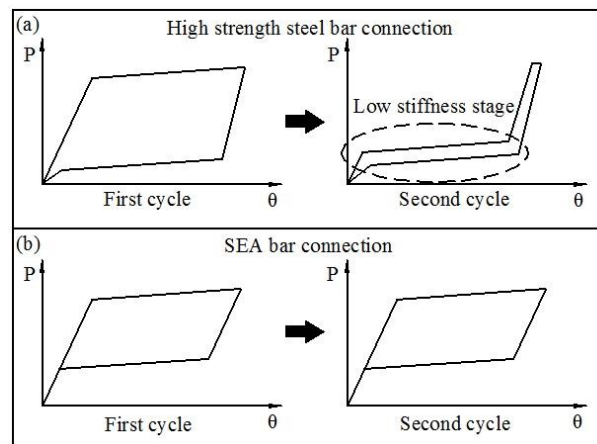
243

244

Figure 17 The second cycle hysteresis loops of Dou-Gon under 10kN dead load



245 In general, the base Dou system with a high strength steel bar connection has a higher ultimate  
 246 strength than those with wood peg or SEA bar connectors, and it has greater secant stiffness as  
 247 well. The reason for the atypical shape of base Dou system with high strength steel bar  
 248 connection are illustrated in Figure 18a. The high strength steel bar connection dissipated more  
 249 energy than SEA bar connection in the first loading cycle. However, in the second loading  
 250 cycle, before the Dou-Gon with high strength steel connection reaches the ultimate strength, it  
 251 needs to undergo a stage with very low tangent stiffness because the steel bar has already  
 252 experienced several loading cycles with smaller rotational angle. The low stiffness comes from  
 253 the structure itself. The high strength steel bar has permanent deformations and with low  
 254 stiffness after first loading cycle called pinching effect. The energy dissipation of SEA bar  
 255 connection has negligible difference between the first two loading cycles. The Dou-Gon with  
 256 high strength steel bar connection was subjected to 3 loading cycles at  $\Delta L = 60\text{mm}$ . The areas  
 257 in the hysteresis loops significantly reduced during the 2<sup>nd</sup> and 3<sup>rd</sup> loading cycles (Figure 19).  
 258 The high strength steel bar fractured before the specimen reached  $\Delta L = 80\text{mm}$ . On the other  
 259 hand, 2 loading cycles were applied to the Dou-Gon system with SEA bar connection at  
 260  $\Delta L = 70\text{mm}$ . During the loading cycles, the shape of hysteresis loops almost remains unchanged  
 261 (Figure 19).



262  
 263 Figure 18 Schematic illustration of first two loadings cycles of Dou-Gon connects by (a) high strength  
 264 steel bar and (b) SMA bar

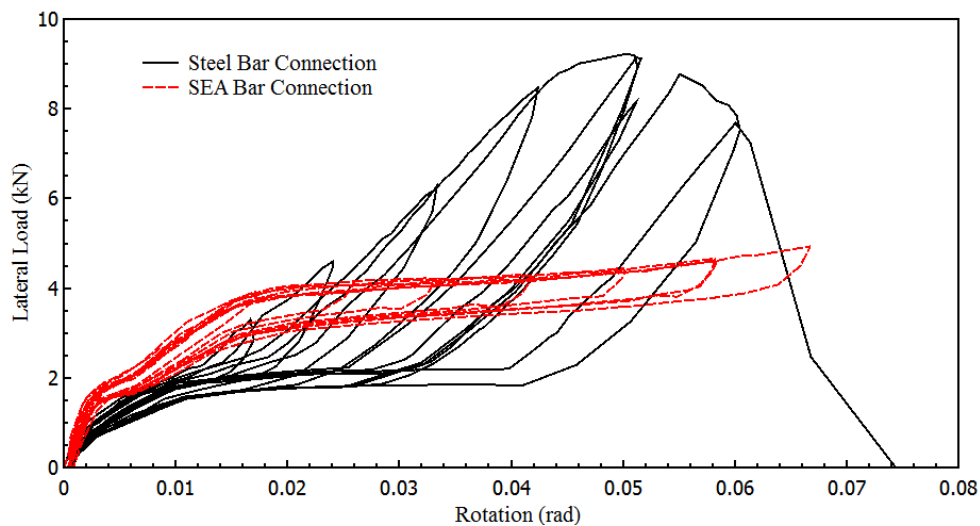
265 Equivalent damping ratios ( $\zeta$ ) for each loading case were calculated by equation:

266 
$$\zeta = \frac{A_h}{4\pi \times A_e} \quad (4)$$

267 where  $A_h$  is the dissipated energy in 1 loading cycle and  $A_e$  is the maximum elastic strain  
 268 energy in 1 loading cycle.

269 The equivalent damping ratio of high strength steel bar connection when  $\Delta L=70\text{mm}$  dropped  
270 from 6.35% to 2.66% and 1.40% at the 2nd and 3rd loading cycles, respectively. The SEA  
271 bar connection gave 4.13% and 4.08% equivalent damping ratios during the 2 loading cycles  
272 at  $\Delta L=70\text{mm}$  as shown in Figure 20. The high strength steel bar connection can only provide  
273 high equivalent damping ratio in the first loading cycle and fractured after few loading  
274 cycles. The SEA bar connection can give a consistent equivalent damping ratio and better  
275 fracture behaviour since there is no fracture has been gathered during the non-prestrain tests.

276 The high strength steel bar connection has permanent deformation after each loading cycle,  
277 which reduces damping capacity while the SMA bar connection gives a consistent damping  
278 behaviour to the Dou-Gon system. Several aftershocks happen after the main shock in an  
279 earthquake. This requires the Dou-Gon system has stable damping ratio to dissipate energy  
280 during the aftershocks as well. The high strength steel bar connections provide low equivalent  
281 damping ratio and small resistance to the Dou-Gon during the aftershocks since they would  
282 have permanent deformations after the main shock. And the SEA bar connections can give  
283 consistent damping behaviour and dissipate energy persistent in both main shock and  
284 aftershocks.

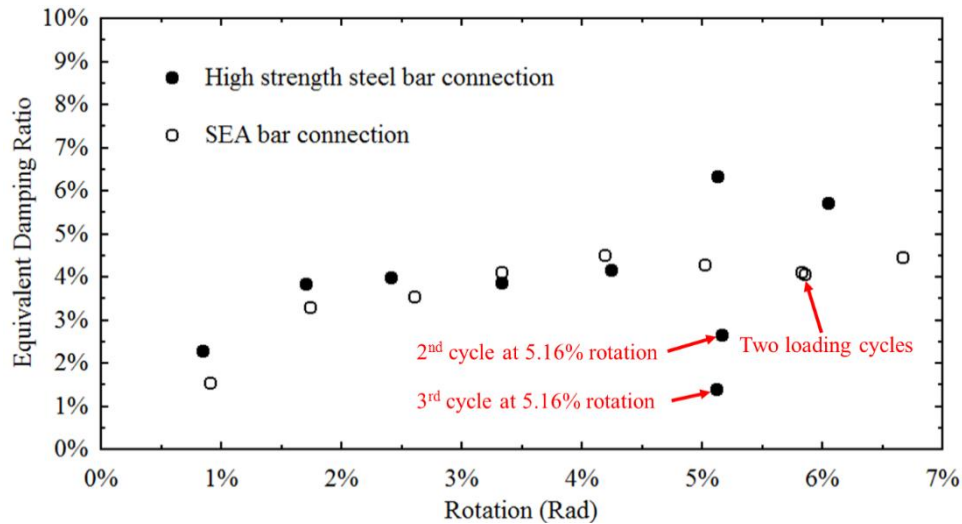


285

286 Figure 19 Hysteresis loop histories of both high strength steel bar and SMA bar connections under

287

10kN vertical loads



288

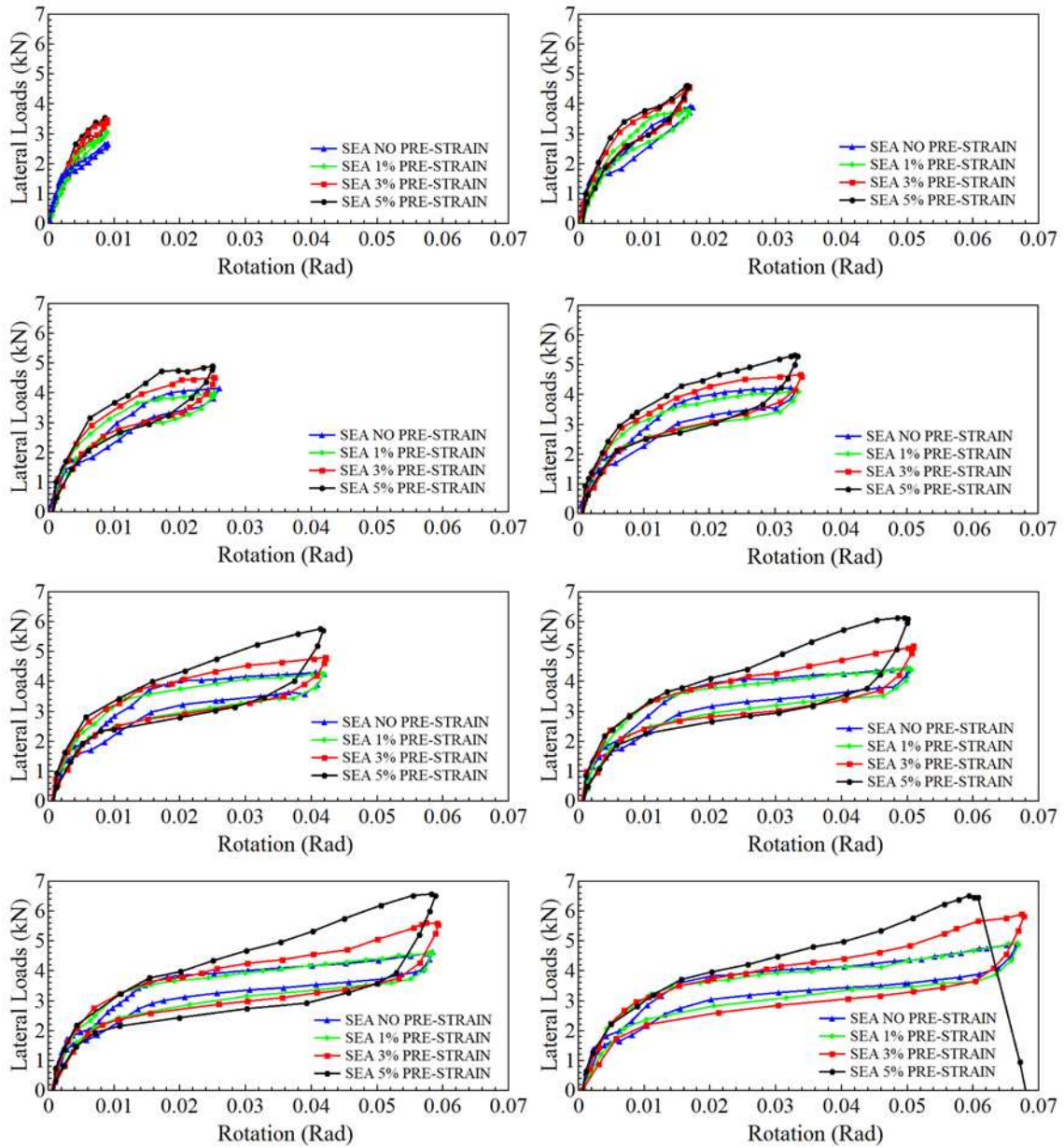
289 Figure 20 Equivalent damping ratios of both high strength steel bar and SMA bar connections under  
 290 10kN vertical loads

291

### 292 4.3. The effects of SMA bar connector with different levels of pre-strain

293 Previous research works showed that the pre-strain of SEA bars will give to the materials a  
 294 larger energy dissipation capacity. In this research, the SEA bar connections was pre-strained  
 295 to 1%, 3% and 5% strain levels, aiming at a higher damping ratio of the base Dou system.

296 Figure 21 illustrates that the SEA bar connector without pre-strain has experienced three stages  
 297 of stiffness variation before the SEA enters the martensitic phase. So, it can only dissipate little  
 298 amount of energy during small rotations. The shape of hysteresis loop of SEA bar with 1% pre-  
 299 strain was not too much different from the one without pre-strain but change to the martensitic  
 300 phase quicker. Because the pre-strain eliminates any possible slack between the structure and  
 301 the connection system, and SEA bar starts to work from the beginning of loading. The ultimate  
 302 strength increased with the increase of the pre-strain level. The lateral load started to rise again  
 303 after 4.5% radians for the SEA bar connection with 3% pre-strain. Because the SEA material  
 304 is at its martensitic phase when it was pre-strained to 5% strain level. The second stiffness of  
 305 SEA bar connection with 5% pre-strain is much higher than others and the lateral load increased  
 306 to nearly 7kN when  $\Delta L=70\text{mm}$  which gives a much better damping capacity than others.  
 307 However, the SEA bar with 5% pre-strain fractured when the structure tried to reach 80mm in  
 308  $\Delta L$ .

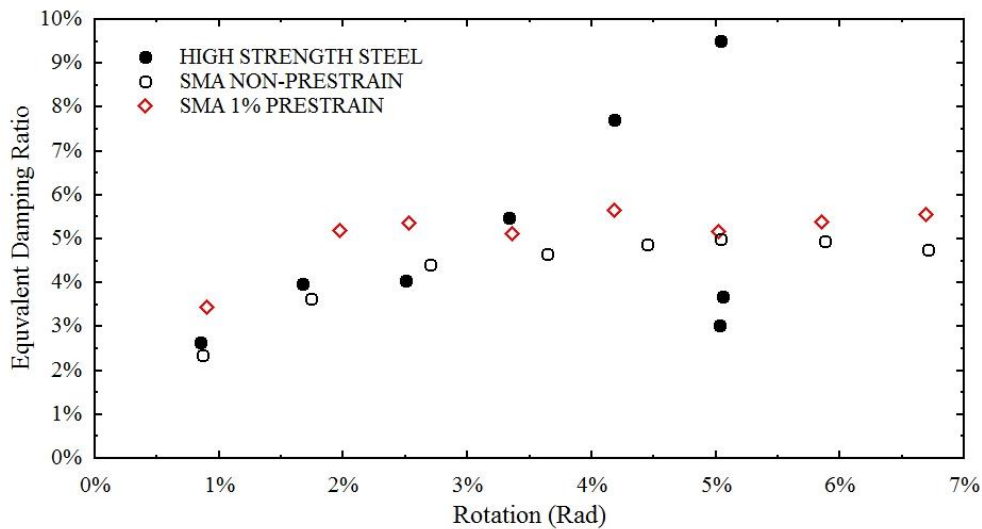


309

310 Figure 21 The hysteresis loops of Dou-Gon with SEA bar connection under 10kN dead load

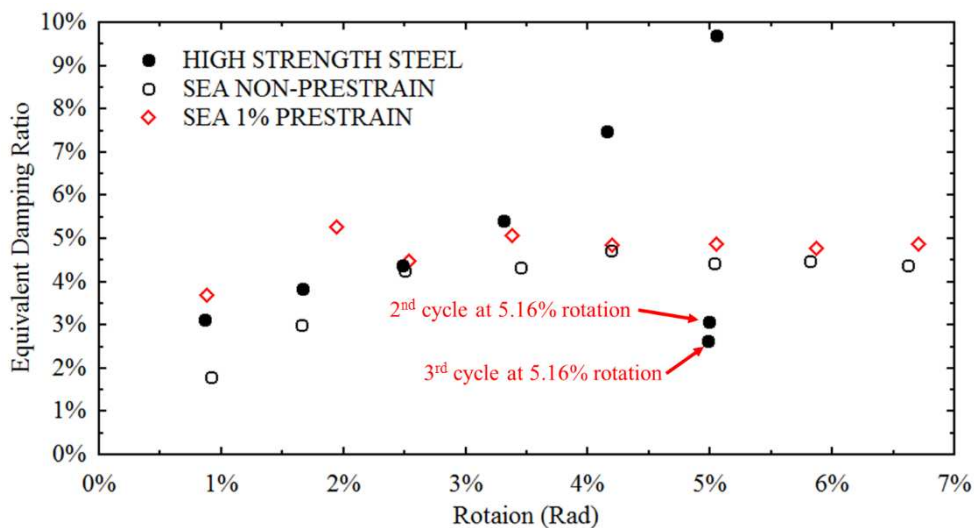
311 Figure 22 and Figure 23 show that, under 4 and 7 kN vertical loads, SEA bar connectors with  
 312 1% pre-strain gave higher equivalent damping ratio than non-prestrain ones during small  
 313 prescribed rotation and become closer when  $\theta$  increases. The equivalent damping ratio of high  
 314 strength steel bar connector increases with the increasing of  $\Delta L$  and SEA bar connector gives  
 315 a constant equivalent damping ratio when  $\Delta L \geq 20\text{mm}$ . The SEA bar connector with 1% pre-  
 316 strain have slightly larger equivalent damping ratio than the one without pre-strain. When  $\Delta L$   
 317  $< 40\text{mm}$ , the high strength steel bar connector has a higher equivalent damping ratio than the  
 318 SEA bar connector without pre-strain but lower than the SEA bar connector with 1% pre-strain.  
 319 They have the similar equivalent damping ratio when  $\Delta L = 40\text{mm}$ . Under  $\Delta L$  equals to 50mm

320 and 60mm, the high strength steel bar connection gives much higher equivalent damping ratios  
 321 than other two connectors, but there are dramatic declines after the first cycle. The fracture  
 322 strain of the high strength steel bar was tested to be  $3.7 \times 10^4 \mu\epsilon$ . The high strength steel bar  
 323 connections fractured when the base Dou system trying to reach 70mm of  $\Delta L$  in both loading  
 324 conditions. The behaviour was almost the same with 10kN vertical loads. No fracture happens  
 325 to the SEA bars during the tests under 4kN and 7kN vertical loads which shows a longer fatigue  
 326 life than high strength steel bar.



327  
 328

Figure 22 Equivalent damping ratios of Dou-Gon under 4kN dead loads

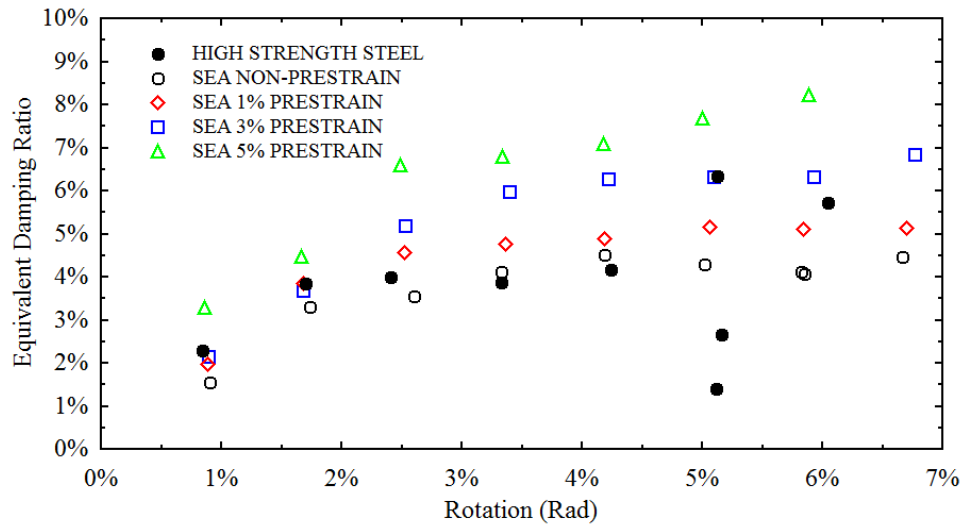


329  
 330  
 331

Figure 23 Equivalent damping ratios of Dou-Gon under 7kN dead loads

332 Under 10kN vertical loads, Figure 24, the equivalent damping ratios of SEA bar connectors  
 333 with pre-strain were always larger than the ones without pre-strain. The equivalent damping

334 ratio is increased as the pre-strain level increased. The SEA bar connector with 5% pre-strain  
 335 gave the highest damping ratio under 10kN vertical loads but fractured when  $\Delta L=80\text{mm}$ . The  
 336 equivalent damping ratio of SEA bar connector with 3% pre-strain increases when  $\Delta L<40\text{mm}$   
 337 and remain constant after that. The SEA bar connector with 5% pre-strain has a rapid increase  
 338 when  $\Delta L<30\text{mm}$  and rise steadily after a plateau of  $\Delta L$  is between 30mm and 50mm.



339

340 Figure 24 Equivalent damping ratios of Dou-Gon under 10kN dead loads

341

## 342 5. Conclusion

343 The Dou-Gon system is the primary element of the historic timber structure in Asia which is  
 344 located on top of a column to transfer the upper loads to the column. The historic timber  
 345 structure has expressed strong seismic performance because Dou-Gon can dissipate significant  
 346 amount of energy due to sliding between wood elements and yielding of wood elements in  
 347 compression perpendicular to the grain. They also have a good re-centring capability since the  
 348 heavy roof gives the re-centring force to the Dou-Gon. However, they have still been damaged  
 349 by earthquake seriously and the seismic performance of historic timber structure needs to be  
 350 enhanced.

351 The conventional connection of the base Dou and column uses a wood peg. In this research, a  
 352 technique has been developed to enhance the seismic performance of a base Dou system that  
 353 duplicate an ancient structure in Sichuan Province in China by using super-elastic alloy and  
 354 high strength steel bars. Pushover tests have been done to the base Dou system with three

355 different connectors (wood peg, high strength steel bars and SEA) under 4kN, 7kN and 10kN  
356 vertical loads.

357 The lateral load that applies on the base Dou system is overcoming the vertical loads when they  
358 are connected by the wood peg, so the ultimate strength of the base Dou system will increase  
359 with the weight of the roof. The high strength steel bar connection has a much higher ultimate  
360 strength than other types of connections, but only in the first loading cycle. For the second and  
361 third loading cycles, the equivalent damping ratio has a dramatic reduction. A consistent  
362 damping performance can be achieved by using the SEA bar connector. The pre-strain of the  
363 SEA bar gives a higher equivalent damping ratio to the base Dou system. The equivalent  
364 damping ratio increases with the pre-strain level of the SEA bar. When the SEA bar has been  
365 pre-strained to 5% strain level, the equivalent damping ratio reached a maximum of 8%. The  
366 SEA bar has a longer fatigue life than the high strength steel bar. In general, the energy  
367 dissipation capacity and ultimate strength of base Dou system have been increased by this  
368 simple technique. SEA bar is more suitable for using in the seismic application since the  
369 constant damping behaviour could overcome both main shock and aftershocks of the  
370 earthquake.

## 371 References

- 372 Araki, Y., Endo, T., Omori, T., Sutou, Y., Koetaka, Y., Kainuma, R. & Ishida, K., 2011. Potential of  
373 superelastic Cu-Al-Mn alloy bars for seismic applications. *Earthquake Engineering and Structural*  
374 *Dynamics*, Volume 40, pp. 107-115.
- 375 Chang, W.-S. & Araki, Y., 2016. Use of shape-memory alloys in construction: a critical review.  
376 *Proceedings of the Institution of Civil Engineers - Civil Engineering*.
- 377 D'Ayala, D. & Tsai, P.-H., 2008. Seismic vulnerability of historic Dieh-Dou timber structures in  
378 Taiwan. *Engineering Structures*, 30(8), pp. 2101-2113.
- 379 Fang, D.-P., Iwasaki, S., Yu, M. H. & Shen, Q. P., 2001. Ancient Chinese timber architecture. I:  
380 Experimental study. *Journal of Structural Engineering*, 127(11), pp. 1348-1357.
- 381 Fang, D. P., Iwasaki, S., Yu, M. H. & Shen, Q. P., 2001. Ancient Chinese Timber Architecture. II:  
382 Dynamic Characteristics. *Journal of Structural Engineering*, Nov.127(11).
- 383 Fujita, K., Sakamoto, I., Ohashi, Y. & Kimura, M., 2000. *Static and dynamic loading tests of bracket*  
384 *complexes used in traditional timber structures in Japan*. New Zeland, 12th World Conference on  
385 Earthquake Engineering.
- 386 Janke, L., Czaderski, C., Motavalli, M. & Ruth, J., 2005. Applications of shape memory alloys in civil  
387 engineering structures--Overview, limits and new ideas. *Materials and Structures*, 38(5), pp. 578-592.
- 388 Kyuke, H., Kusunoki, T., Yamamoto, M., Minewaki, S. & Kibayashi, M., 2008. *Shaking Table Tests*  
389 *of 'MASUGUMI' Used in Traditional Wooden Architectures*. Miyazaki, s.n.
- 390 Omori, T. & Kainuma, R., 2013. Alloys with long memories. *Nature*, 502(7469), pp. 42-44.



- 391 Omori, T., Kusama, T., Kawata, S., Ohnuma, I., Sutou, Y. Araki, Y., Ishida, K. & Kainuma, R., 2013.  
392 Abnormal grain growth induced by cyclic heat treatment. *Science*, Volume 341, pp. 1500-1502.
- 393 Suzuki, Y. & Maeno, M., 2006. Structural mechanism of traditional wooden frames by dynamic and  
394 static tests. *Structural Control and Health Monitoring*, Volume 13, pp. 508-522.
- 395 Tsai, P.-H. & D'Ayala, D., 2011. Performance-based seismic assessment method for Taiwanese  
396 historic Dieh-Dou timber structures. *Earthquake Engineering and Structural Dynamics*, Volume 40,  
397 pp. 709-729.
- 398 Tsuwa, I., Koshihara, M., Fujita, K. & Sakamoto, I., 2008. *A Study on the Size Effect of Bracket*  
399 *Complexes Used in Traditional Timber Structures on the Vibration Characteristics*. Miyazaki, s.n.,  
400 pp. 1344-1351.
- 401 Xue, J., Wu, Z., Zhang, F. & Zhao, H., 2015. Seismic Damage Evaluation Model of Chinese Ancient  
402 Timber Buildings. *Advances in Structural Engineering*, 7 Nov, 18(10), pp. 1671-1683.
- 403 Yeo S.-Y., Hsu, M.-F., Komatsu, K., Chung, Y.-L. & Chang, W.-S., 2016. Shaking Table Test of the  
404 Taiwanese Traditional Dieh-Dou Timber Frame. *International Journal of Architectural Heritage:*  
405 *Conservation, Analysis, and Restoration* , 10(5), pp. 539-557.
- 406 Yeo, S.-Y., Komatsu, K., Hsu, M.-F. & Que, Z., 2016. Mechanical model for complex brackets  
407 system of the Taiwanese traditional Dieh-Dou timber structures. *Advances in Structural Engineering*,  
408 19(1), pp. 65-85.
- 409 Yu, M.-H., Oda, Y., Fang, D.-P. & Zhao, J.-H., 2008. Advances in structural mechanics of Chinese  
410 ancient architectures. *Frontiers of Structural and Civil Engineering*, 2(1), pp. 1-25.
- 411